

Adaptive Deep Learning for Multiclass Breast Cancer Classification via Misprediction Risk Analysis

Gul Sheeraz^a, Qun Chen^b, Liu Feiyu^c, Zhou Fengjin, MD^d

^a*School of Computer Science, Northwestern Polytechnical University, , Xian, , Shaanxi, China*

^b*School of Computer Science,, Northwestern Polytechnical University, , Xian, , Shaanxi, China*

^c*School of Software, Northwestern Polytechnical University, , Xian, , Shaanxi, China*

^d*Honghui Hospital, Xian Jiao Tong Universtiy, , Xian, , Shaanxi, China*

Abstract

Breast cancer remains one of the leading causes of cancer-related deaths worldwide. Early detection is crucial for improving patient outcomes, yet the diagnostic process is often complex and prone to inconsistencies among pathologists. Computer-aided diagnostic approaches have significantly enhanced breast cancer detection, particularly in binary classification (benign vs. malignant). However, these methods face challenges in multiclass classification, leading to frequent mispredictions. In this work, we propose a novel adaptive learning approach for multiclass breast cancer classification using H&E-stained histopathology images. First, we introduce a misprediction risk analysis framework that quantifies and ranks the likelihood of an image being mislabeled by a classifier. This framework leverages an interpretable risk model that requires only a small number of labeled samples for training. Next, we present an adaptive learning strategy that fine-tunes classifiers based on the specific characteristics of a given dataset. This approach minimizes misprediction risk, allowing the classifier to adapt effectively to the target workload. We evaluate our proposed solutions on real benchmark datasets, demonstrating that our risk analysis framework more accurately identifies mispredictions compared to existing methods. Furthermore, our adaptive learning approach significantly improves the performance of state-of-the-art deep neural network classifiers.

Keywords: Breast Cancer Detection, Risk Analysis, Misprediction, Multiclass Classification, Adaptive Training

1. Introduction

Breast cancer, with over 2.3 million cases annually, stands as the most prevalent adult cancer, and globally, it is the leading or second leading cause of cancer-related deaths in 95% of countries [31, 12]. Timely detection is crucial to reducing mortality rates in breast cancer-related deaths. The detection of breast cancer, a heterogeneous collection of diseases arising from epithelial tissue abnormalities, requires various radiological approaches (e.g., Mammography, Ultrasound, MRI) [48, 43]. However, these methods may not fully capture heterogeneity. Histopathological studies, including biopsy and microscopic examination, offer in-depth information on breast tissue characteristics [11, 4].

Histopathological images of breast tumors contain crucial information such as tumor type and cancer stage. However, manual analysis by experienced pathologists is time-consuming. A study indicates a notable misdiagnosis rate, with 1 in 71 biopsies and 1 in 5 cancer cases being misclassified [47]. Computer-Aided Diagnosis aids in accurate diagnosis, especially in binary classification [50]. Recent advances in AI have introduced state-of-the-art approaches [39, 9, 22, 1, 25], predominantly using deep learning and convolutional neural networks (CNN) for optimal performance on both binary and multiclass classification. However, these DNN models may still struggle in real scenarios, where a limited amount of training data are provided. In this case, a well-trained model can not perform satisfactorily due to data distribution shift, and mispredictions are a common occurring. Challenges particularly arise in multiclass classification due to inter-class consistency and variability.

In this paper, we propose to enable adaptive deep learning for multiclass classification of breast cancer based on H&E-stained histopathological images via misprediction risk analysis. We first present a novel solution for multiclass risk analysis, which can effectively quantify an image’s misprediction risk by a DNN model. As shown in Figure 1, utilizing knowledge from the existing risk analysis framework i.e LearnRisk, which currently handles binary classification tasks. Our proposed solution MultiRisk, consists of novel risk feature generation for multiclass, an attention-based risk model construction and optimized training for multiclass, and a risk-based adaptive training approach for multicalss classification of breast cancer. Risk feature generation involves a fusion-based strategy that combines the advantages of feature selection,

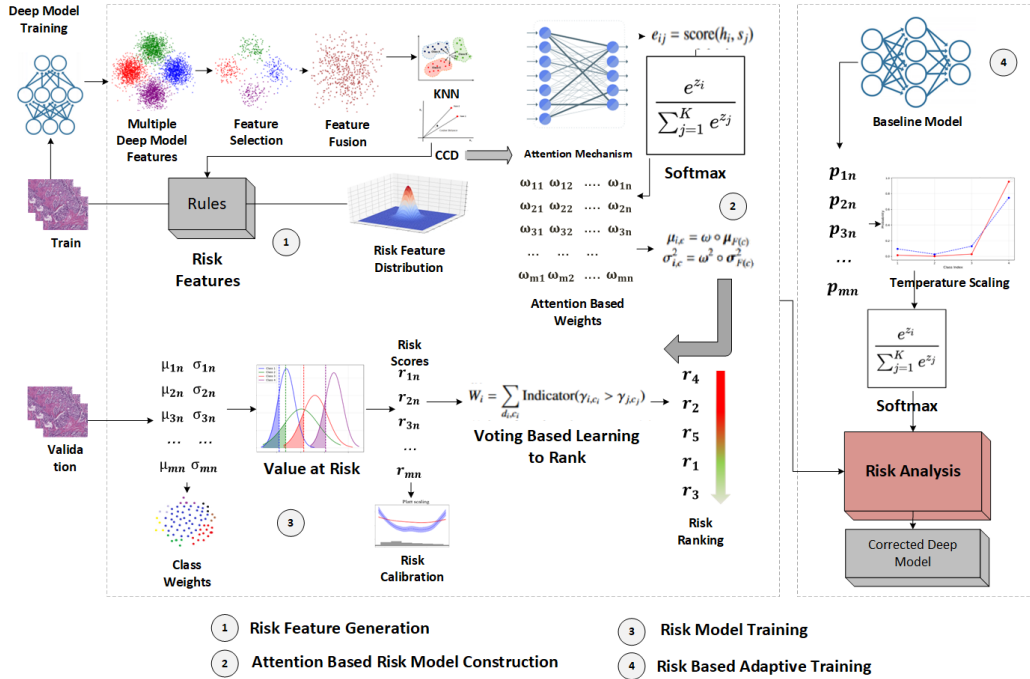


Figure 1: Misprediction Risk Analysis for Multiclass Classification of Breast Cancer

diverse risk metrics extraction, and multiclass decision tree rule generation, resulting in diverse risk features. A risk model is constructed using an attention mechanism and class based structure to target all classes in a multi-class scenario. Risk model training starts by balancing classes on expectation and variance by refining the class frequency bias, after calculating the VaR metric a risk calibration is then applied to mitigate the overfitting in Risk analysis, and finally a voting-based learning to rank objective for multiclass to rank images based on the risk of each class. Finally, after identifying the mispredictions, a risk-based adaptive training approach effectively fine-tunes a DNN model towards a new workload based on its particular characteristics taking a temperature scaling-based calibrated model output as input. This approach achieves adaptation with only a few labeled new training data by minimizing a classifier’s misprediction risk on the new workload.

The main contributions of this paper are summarized as:

1. We propose a novel approach to misprediction risk analysis for multiclass breast cancer classification. Instead of building a separate risk model for each class, as in the binary case, our method constructs a

unified risk model for all classes by leveraging diverse features extracted from multiple deep neural network (DNN) architectures.

2. We introduce an attention-based risk model along with a corresponding training strategy that refines class biases and calibrates scores for improved multiclass performance. Additionally, the model ranks instances using a voting-based strategy to enhance the accuracy of risk model training.
3. We propose a novel adaptive deep learning solution via risk analysis for multiclass breast cancer classification. This method dynamically fine-tunes the model for a specific workload by minimizing misprediction risk through a two-phase approach: a pre-training phase followed by risk-based adaptive training.
4. We conduct an extensive empirical study to validate the effectiveness of our proposed solutions. Experiments on real breast cancer benchmark datasets demonstrate that our risk analysis method outperforms existing approaches in identifying mispredictions, while the adaptive training approach surpasses state-of-the-art models in multiclass breast cancer classification.

2. Related Work

In the field of multiclass classification of breast cancer, recent advancements in image analysis and computer-aided diagnosis have been dominated by deep learning, especially convolutional neural networks (CNNs) [37, 2, 5, 18, 46, 28, 41, 3, 6]. Customized CNN architectures like ResHist, BreastNet, and hybrid CNN-RNN models have achieved notable accuracies, often fine-tuned on pretrained models such as VGG16 and Inception-V3. Benchmark datasets like BACH [3] and BRACS [6] have played a crucial role in standardizing evaluation metrics and facilitating the development of tailored models. While deep CNN architectures remain state-of-the-art, the field continues to evolve with the exploration of vision transformers and hierarchical graph networks [40, 32].

In the context of adaptive deep learning, various approaches have been proposed, where most of them adapt a deep model towards a target workload overcoming distribution misalignment between training and target data. Two primary strategies, transfer learning and adaptive representation learning data [52, 35, 14, 36, 23], address this issue. Transfer learning aims to adapt a model from a source domain to perform well on a target domain, while adaptive representation learning focuses on learning domain-invariant

features shared across diverse domains. Despite their effectiveness, existing approaches often struggle to fine-tune deep models for new workloads with specific characteristics. In image classification domain adaptation, recent methods like SCDA (Semantic Concentration for Domain Adaptation) [24], and TSA (Transferable Semantic Augmentation) [23] target distribution alignment and feature augmentation respectively. These strategies can be adapted for various medical image analysis challenges. Moreover, using misprediction risk analysis in adaptive deep learning, as demonstrated in tasks like entity resolution [8, 29] and network intrusion detection [51], remains a valuable direction.

Analyzing misprediction risk, also known as "confidence ranking" or "trust scoring," has been a key focus [16, 19, 8, 30]. Early approaches relied on softmax distributions to identify misclassified instances. More recently, the LearnRisk framework has emerged as an interpretable and trainable solution for risk analysis. Notably, our work extends LearnRisk’s application from entity resolution to the domain of multiclass breast cancer classification, introducing several important strategies.

3. Preliminaries

3.1. Problem Statement

The task of multi-class breast cancer classification involves assigning breast tissue images to one of several predefined categories. Given a dataset $\mathcal{D} = \{(\mathbf{x}_i, y_i)\}_{i=1}^N$, the objective is to train a model M that accurately predicts the class label $y \in \{1, 2, \dots, C\}$ for feature \mathbf{x} while minimizing classification errors. Complementing this, misprediction risk analysis focuses on assessing the likelihood of errors in the predictive model M . By generating risk features and constructing a risk model, the goal is to provide a calibrated risk score r that quantifies the probability of misclassification, enhancing model’s reliability and supporting clinical decision-making.

The purpose of this work is to create a misprediction risk analysis framework which can effectively identify the mispredictions from a multiclass output. The primary goal of this work is to utilize a classifier model M to detect and classify H&E-stained histopathological breast tissue images into multiclass categories such as: Normal, Pathological Benign, Usual Ductal Hyperplasia, Flat Epithelial Atypia, Atypical Ductal Hyperplasia, Ductal Carcinoma In Situ, and Invasive Carcinoma further grouped into three broader categories: Benign, Atypical, and Malignant. The dataset D consists of labeled training instances (D_s), labeled validation instances (D_v), and unlabeled target instances (D_t). The focus of misprediction risk analysis is on

evaluating the potential misclassifications of unlabeled target instances (D_t) across various cancer subtypes. This analysis involves ranking mispredicted pairs (x_i^t, y_i^t) before correctly predicted pairs, where x_i^t represents the image and y_i^t is its associated label. The classifier M is informed about mispredictions through a risk ranking list. Evaluation metrics such as the Receiver Operating Characteristic (ROC) and the Area Under the ROC Curve (AUROC) are utilized, with the ultimate goal of maximizing the ROC metric by considering True Positive (TP), True Negative (TN), False Positive (FP), and False Negative (FN) metrics. This comprehensive approach aims to enhance the understanding of misprediction risks and improve the overall performance of the classification model.

3.2. The LearnRisk Framework

The LearnRisk framework is designed to address the challenges of risk analysis in binary classification, particularly for task of Entity Resolution. The framework operates in three key steps: **risk feature generation**, **risk model construction**, and **risk model training**.

The first step, **risk feature generation**, involves evaluating mislabeling risks based on extracted features that satisfy three critical criteria: they must be interpretable, discriminating, and high-coverage. For instance, risk features should be easily understood by humans, clearly differentiate between true labels, and generalize well across data pairs to ensure effective transfer from training to test data. However, applying LearnRisk to multiclass problems introduces challenges, such as generating quality risk features when dissimilar images (e.g., benign vs. tumor subtypes) are grouped together or when imbalanced data complicates feature generation. Overcoming these challenges is vital for multiclass tasks, such as breast cancer classification, where features like embedding distances might indicate risk but lack clarity in handling cases beyond specific thresholds.

Next, in **risk model construction**, the framework models equivalence probabilities for each image pair based on its risk features. Inspired by portfolio investment theory, LearnRisk treats each risk feature as a stock and each pair as a portfolio. The equivalence probability distribution for a labeled pair is represented as $N(\mu_i, \sigma_i^2)$, where μ_i is the expectation and σ_i^2 is the variance. These distributions are truncated to ensure probabilities lie between 0 and 1. The framework utilizes feature weights $w = [w_1, w_2, \dots, w_m]^T$ and feature equivalence probability distributions $N(\mu_{f_j}, \sigma_{f_j}^2)$. The expectation and variance vectors are $\mu_F = [\mu_{f_1}, \mu_{f_2}, \dots, \mu_{f_m}]^T$ and $\sigma_F^2 = [\sigma_{f_1}^2, \sigma_{f_2}^2, \dots, \sigma_{f_m}^2]^T$. For

each pair d_i , with feature vector $x_i = [x_{i1}, x_{i2}, \dots, x_{im}]$, the distribution is defined as:

$$\mu_i = x_i(w \circ \mu_F), \quad (1)$$

$$\sigma_i^2 = x_i(w^2 \circ \sigma_F^2), \quad (2)$$

where \circ denotes element-wise product. Value at Risk (VaR) [21] is then employed to rank pairs based on mislabeling risks, using both expectation and variance to capture the risk of mispredictions effectively.

Finally, **risk model training** fine-tunes the parameters of the risk model to align with the characteristics of breast cancer detection. This step uses a learning-to-rank approach to rank labeled pairs by their mislabeling risk. The model parameters include feature weights (w_i), the expectation (μ_i), and the variance (σ_i^2) of the risk feature distribution. The expectation is estimated from labeled data, while weights and variances are tuned during training to optimize risk ranking. The training process uses both target workload data (e.g., breast cancer detection datasets) and validation data to ensure the model captures task-specific characteristics effectively.

4. Multi-class Risk Analysis Solution

In this section, we present the solution of risk analysis for multi-class breast cancer classification. The proposed solution fulfills the core functions of risk analysis laid out in the LearnRisk framework with very important distinctive technical characteristics to make the solution work for multi-class classification

4.1. Risk Feature Generation

If we consider the binary classification example for the breast cancer in terms of risk feature generation, we need to classify the mappings between images in labeled training data and the categories and for the binary cancer classification the categories or classes are ‘Not Cancerous’ (0) and ‘Cancerous’ (1), i.e. negative or positive. For example we have two images shown in table 1:

Image	True Label	Prediction
1	Not Cancerous (0)	Not Cancerous (0)
2	Not Cancerous (0)	Cancerous (1)

Table 1: True Labels and Predictions for Binary Classification

Here, **Image 1** is considered a negative sample, meaning it is not risky, while **Image 2** is considered a positive (i.e., risky) sample. The straightforward *LearnRisk* solution uses a one-hot encoding scheme, mapping samples to either positive or negative values. However, this binary approach is inadequate for multiclass problems. If we directly apply the *LearnRisk* solution to a multiclass task, we must mark positive and negative samples and train a separate risk model for each class.

In the multiclass scenario, all samples with ground-truth labels different from the target label would be grouped into a single category. However, these samples may share very limited similarity, making wholesale risk analysis on them inaccurate. Moreover, the binary approach typically results in **imbalanced samples**, with far fewer risky samples than non-risky ones, further complicating risk analysis.

To address this challenge in multiclass breast cancer classification (e.g., with seven classes), we propose marking each ⟨sample, label⟩ pair as either *Match* or *Unmatch*. As a result, each sample has **one Match pair** and **multiple Unmatch pairs**. Risk features are then generated based on these Match and Unmatch pairs. A unified risk model is subsequently constructed using these risk features to quantify the risk of machine predictions more effectively.

To tackle challenges in multiclass breast cancer detection, we developed a solution for risk feature generation that optimizes multi-class model performance while ensuring high coverage and interpretability. We have sketched the full workflow of risk feature generation in Algorithm 1, whose technical details will be described next.

In our solution, we utilize multiple DNN models to extract diverse features, while enhancing representation, that can also lead to data ambiguity and overfitting, especially in multiclass scenarios where features are often correlated and redundant. To mitigate these challenges, we implement two correlation-based feature selection techniques: Mutual Information [7] and F-Score [15]. Mutual Information quantifies the dependence between features X and the target variable Y as defined by Equation 3:

$$I(X; Y) = \sum_{x \in X} \sum_{y \in Y} p(x, y) \log \left(\frac{p(x, y)}{p(x)p(y)} \right) \quad (3)$$

where $p(x, y)$ is the joint probability distribution of X and Y , and $p(x)$ and $p(y)$ are the marginal probability distributions of X and Y , respectively. The

Algorithm 1 Multiclass Risk Feature Generation

Input: Dataset D and Model Architecture M

Output: Risk features for breast cancer dataset in the form of rules

```
1: procedure FUSIONBASEDRISKFEATUREGEN
2:   Train models  $M$  (CNNs, Transformer) on Dataset  $D$ 
3:   for each image  $I$  in  $D$  do
4:     Extract features using the trained Deep Models.
5:     Apply feature selection (MI, FS).
6:     Fuse the features along y-axis for each label.
7:     Calculate risk metrics (CCD, KNN).
8:   end for
9:   Map images to categories (M/U) based on true/predicted labels.
10:  for  $i$  in range( $m$ ) do
11:    Generate one sided decision tree rules.
12:    Generate risk features using the mappings and rules with fused
    features.
13:  end for
14: end procedure
```

F-score assesses feature discriminative power by comparing variance between and within classes, as shown in Equation 4:

$$F(f_i) = \frac{\sum_j (\mu_i - \mu_{i,j})^2}{\sum_j \sigma_{i,j}^2} \quad (4)$$

where μ_i is the overall mean of feature f_i , $\mu_{i,j}$ is the mean of feature f_i within class j , and $\sigma_{i,j}^2$ is the variance of feature f_i within class j . For example, in feature selection from ResNet50, let $\mathbf{f}_{\text{ResNet50}} \in \mathbb{R}^d$ be the output feature vector. We define selection functions:

$$F_{\text{MI}}(\mathbf{f}_{\text{ResNet50}}) = \text{Top}_{200}(I(\mathbf{f}_{\text{ResNet50}}; Y)) \quad (5)$$

$$F_{\text{FS}}(\mathbf{f}_{\text{ResNet50}}) = \text{Top}_{200}(F(\mathbf{f}_{\text{ResNet50}})) \quad (6)$$

where $I(\mathbf{f}_{\text{ResNet50}}; Y)$ is the Mutual Information between the feature vector and target labels, $F(\mathbf{f}_{\text{ResNet50}})$ represents the F-score of the feature vector, and Top_{200} selects the top 200 features based on their respective scores.

Finally, we perform feature fusion via concatenation of selected features from multiple models and both feature selections, resulting in:

$$\mathbf{F}_{\text{Fused}} = [\mathbf{f}_{M_1}, \mathbf{f}_{M_2}, \dots, \mathbf{f}_{M_i}], \quad (7)$$

where M_i denotes a DNN model and f_{M_i} denotes the selected features of M_i .

Based on the results of feature fusion on an image’s vector representation we extract two risk metrics of category similarity:

- **Category Cosine Distance (CCD):** We estimate the class center of each category by its representatives in the training data. For a given image, we measure its similarity with each category by calculating the distance to the class centroid, defined as 1.0– vector cosine similarity. A smaller distance indicates a higher probability that the image belongs to the category. This metric is denoted as *CCD* shown in equation 8:

$$\text{CCD} = 1 - \cos(\theta), \quad \text{where} \quad \cos(\theta) = \frac{\mathbf{v} \cdot \mathbf{c}}{\|\mathbf{v}\| \|\mathbf{c}\|} \quad (8)$$

where v is the query vector, c is the class centroid vector, and $\cos(\theta)$ is the cosine similarity between them.

- **K-nearest Neighborhood (KNN):** For each image, we identify the categories of its k -nearest neighbors in an embedding space, where nearness is determined by vector cosine similarity. The effectiveness of this metric relies on the assumption that images appearing close in an embedding space likely share the same label. In our approach, we use different values of K (e.g., $K = 5$ or $K = 7$) to derive distinct risk metrics. With $K = 5$, we consider only the nearest neighbor; with $K = 7$, we include a broader set of representative samples from the local neighborhood. This metric is denoted as *KNN* as shown in equation 9:

$$\mathcal{K}_{\text{NN}} = \{\mathbf{c}_i \mid i \in \operatorname{argmin}_{j \in \{1, 2, \dots, N\}} \|\mathbf{v} - \mathbf{v}_j\|, j = 1, \dots, k\}, \quad (9)$$

where, v is the query vector, v_j is the vector in the embedding space, c_i is the corresponding category, and k is the number of nearest neighbors.

To generate unified risk features, we construct the mappings between images in labeled training data and their corresponding categories (classes) by categorizing them as Matching (M) or Unmatching (U), where for each

Table 2: Example mappings between images and categories. FF represents the Fused Features, CCD category cosine risk metric, KNN(5) denotes the KNN risk metric with $K = 5$, while KNN(7) denotes the KNN risk metric with $K = 7$.

Image	True Label	Category	M/U	FF-CCD	FF-KNN(5)	FF-KNN(7)
d_1	0	Positive	M	0.06	5	7
	0	Negative	U	0.53	0	0
d_2	1	Positive	U	0.57	1	2
	1	Negative	M	0.04	4	5
d_3	2	Positive	M	0.07	4	6
	2	Negative	U	0.63	1	1
d_4	3	Positive	U	0.80	2	3
	3	Negative	M	0.02	3	4

image there is one M and all other are U. An illustrative mapping table has been shown in Table 2. Leveraging this mapping information. One-sided decision trees will then be employed to extract risk features (rules) based on these mappings. The rules are generated using thresholds on risk metrics, where each partitioning focuses on maximizing the "purity" of either the Matching (M) or Unmatching (U) sets.

This process mirrors the binary one sided decision tree rule generation, but it is adapted for multiclass settings by ensuring that each image's classification is evaluated against all possible class labels. The technical details for decision tree rules of this process align with prior work [8]. These rules operate on conditions and thresholds involving the risk metrics. It should be mentioned here that M/U targets the predicted class of an image. An illustrative example 4.1 of risk feature is shown as follows:

Example 4.1. *Suppose a one sided decision tree rule based risk feature is expressed as:*

$$d_1[FF - CCD] < 0.11 \rightarrow M \quad (10)$$

here, d_1 represents an image, CCD is the category cosine distance metric, and $d_1[FF - CCD]$ denotes the image's cosine distance to a class centroid based on the Fused features. This rule implies that if an image, according to the Feature FF , is very close to a class center but has a machine label different from the class, it is considered at high risk of misprediction. However, it's essential to note that this rule does not indicate any category preference if the measured distance exceeds 0.11. Valid risk features, represented as rules, are statistically satisfied by a high percentage (e.g., 95%) of instances in the training data mapping table.

Table 3: Examples of generated risk features on the BRACS Breast Cancer Dataset.

Rule	Description
r_1 : FF - 0 - CCD $\leq 0.104 \rightarrow M$	r_2 : FF- 1 - CCD $> 0.359 \rightarrow U$
r_3 : FF - 0 - KNN5 $> 4.5 \rightarrow M$	r_4 : FF - 2 - KNN5 $\leq 0.5 \rightarrow U$
r_5 : FF - 0 - KNN7 $> 6.5 \rightarrow M$	r_6 : FF - 3 - KNN7 $\leq 0.5 \rightarrow U$

More examples of one-sided rules generated on the BRACS benchmark dataset [6] are presented in Table 3, in which some of the examples have also been described in example 4.2:

Example 4.2. *Let’s take r_1 , r_2 , and r_5 as examples. r_1 shows if the CCD distance for the FF less than or equal to 0.104, then it is a match (M) w.r.t whatever predicted label of an image. r_2 shows that if the CCD distance for the FF feature is greater than 0.359, then it’s an unmatched (U), which means in this scenario, it doesn’t belong to a predicted label.*

4.2. Attention-based Risk Model Construction

The existing binary model supposes risk features are mutually independent. However, in real scenarios, risk features are to a large extent correlated, which is especially true in the multi-class scenario. Therefore, we present a new dynamic risk model with attention-based weighting for multi-class risk analysis. The attention mechanism dynamically adjusts the importance of risk features based on the context of each class, improving multiclass classification by weighting features according to their relevance [42, 26].

Unlike the static methods of Gaussian weighting proposed for binary analysis, the proposed risk model assigns context-specific weights, enabling the model to emphasize informative data and reduce irrelevant information. The structure of the attention-based risk model has been presented in Figure 2. To implement the attention mechanism, we add a linear layer to the model to enable dynamic and context-sensitive feature weighting. The linear layer learns to transform the input features $\mathbf{x} \in \mathbb{R}^{\text{input-dim}}$ into class-specific scores. These scores are represented as:

$$e_{ij} = \text{score}(h_i, s_j), \tag{11}$$

where h_i is the hidden state of the input sequence at position i and s_j is the hidden state of the output sequence at position j . We then align these scores

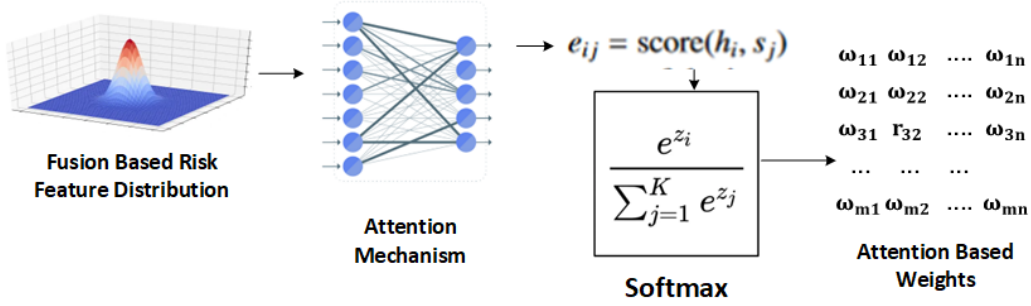


Figure 2: Attention Based Risk Model

using the softmax function:

$$\omega_{ij} = \frac{\exp(e_{ij})}{\sum_{k=1}^n \exp(e_{ik})} \quad (12)$$

where ω_{ij} represents the alignment score, obtained using the softmax function to normalize the scores across all input positions, which gives us the attention-based weights. Finally, we obtain context-aware expectation and variance vectors. Accordingly, the distribution of an image d_i is estimated by the context-aware vectors:

$$\mu_i = \omega \circ \boldsymbol{\mu}_F \quad (13)$$

$$\sigma_i^2 = \omega^2 \circ \boldsymbol{\sigma}_F^2 \quad (14)$$

where ω represents the attention weights, μ and σ^2 represents the expectation and variance, and \circ represents the element-wise product. Different classes may require attention to different features or parts of the input. An attention mechanism can learn to focus on the most informative features for each class dynamically, improving the model's ability to differentiate between classes.

Example 4.3. *In a multi-class classification task, consider an image d_i that can belong to one of four classes: A , B , C , or D . In the learnable Gaussian model, each class has a set of mean $(\mu_A, \mu_B, \mu_C, \mu_D)$ and variance $(\sigma_A^2, \sigma_B^2, \sigma_C^2, \sigma_D^2)$ parameters that are learned from the risk features. These parameters are used to compute the Gaussian weights, however, even with these learnable parameters, the model still uses fixed, class-specific parameters that do not change dynamically based on the image content. In contrast,*

the attention mechanism assigns dynamic weights based on the risk features. For example, for image d_i , the attention mechanism might assign $\omega_A = 0.6$, $\omega_B = 0.1$, $\omega_C = 0.2$, and $\omega_D = 0.1$, emphasizing class A more than the others based on the image’s specific features. This dynamic adjustment allows the attention mechanism to focus on the most relevant classes for each input image, whereas the Gaussian model is constrained by pre-learned, static parameters.

4.3. Risk Model Training

For risk model training, our proposed approach considers the expectation (μ_i) as prior knowledge, which can be estimated based on the labeled training data, and fine-tunes the variances ($\sigma_{i,c}^2$) and feature weights (ω_i) to differentiate between correctly and incorrectly labeled samples. We have sketched the algorithm for risk model training in Alg 2.

Class imbalance is common in most histopathology image datasets, as shown in Tables 4 and 5, particularly in the training data. To address this issue, we propose to neutralize class bias in expectation and variance for balanced learning and prediction. The neutralization operation is formally defined by Equation 15, and 16 as follows:

$$\mu_i = \text{softmax}(\mu_{\text{raw},i} - w_i) \quad (15)$$

$$\sigma_i^2 = \sigma_{\text{raw},i}^2 - \alpha \cdot w_i \quad (16)$$

where $\mu_{\text{raw},i}$ and $\sigma_{\text{raw},i}^2$ represent the raw expectation and variance values, w_i the class weights, and α the scaling factor. The adjusted expectations μ_i are then normalized using the softmax function.

Furthermore, compared to binary risk analysis, where there are only two candidate classes, the multi-class scenario usually has less labeled data for risk model training for each class. To address ineffectiveness of labeled training data and class imbalance, we use Platt Scaling calibration to adjust classifier overconfidence [49] as follows:

$$P(y = k | x) = \frac{1}{1 + \exp(A_k \cdot f_k(x) + B_k)} \quad (17)$$

where $P(y = k | x)$ is the probability of class k given input x , $f_k(x)$ is the output score of the classifier for class k , and A_k, B_k are calibration parameters learned during the Platt Scaling process. Calibration enhances decision

accuracy by aligning predicted risk with actual outcomes, using class-specific parameters A_k and B_k along with the raw score $f_k(x)$.

Algorithm 2 Multiclass Risk Model Training

Require:

- 1: Positive Samples
- 2: Pairs of data and their respective classes: $(d_i, c_i), (d_j, c_j)$
- 3: Initial expectations and variances for each class: $\mu_{i,c}, \sigma_{i,c}^2$
- 4: VaR risk values for each class: VaR_c
- 5: Learning rate η
- 6: Maximum number of training iterations N

Ensure:

- 7: Updated expectations $\mu_{i,c}$, variances $\sigma_{i,c}^2$, attention weights ω , class weights w , and Risk Calibration
- 8: **for** $i = 1$ to N **do**
- 9: Calculate Attention-based Weights ω_{ij}
- 10: Update Context-aware Expectation and Variance: $\mu_{i,c} \leftarrow \omega \circ \boldsymbol{\mu}_F(c)$, $\sigma_{i,c}^2 \leftarrow \omega^2 \circ \boldsymbol{\sigma}_F^2(c)$
- 11: Neutralize Class Bias: $\mu_i = \mu_{\text{raw},i} - w_i$, $\sigma_i^2 = \sigma_{\text{raw},i}^2 - \alpha \cdot w_i$
- 12: Risk Calibration using platt scaling: $1 + \exp(A_k \cdot f_k(x) + B_k)$
- 13: **Learning to Rank:**
- 14: Calculate the desired target probability $\bar{p}_{ij,c}$
- 15: Calculate the posterior probability $p_{ij,c}$
- 16: Voting based Ranking:

$$W_i = \sum_{d_i, c_i} \text{Indicator}(\gamma_{i,c_i} > \gamma_{j,c_j})$$

- 17: Calculate the loss using aggregated scores $L(D_\gamma)$
 - 18: **end for**
 - 19: Calculate the final loss $L(D_\gamma)$
 - 20: **return** Risk Ranking List
-

In multiclass risk analysis, given two images, d_i and d_j , and the mislabeling risk of (d_i, c_i) and (d_j, c_j) , is γ_{i,c_i} and γ_{j,c_j} , the ranking notation can be denoted as:

$$(d_i, c_i) \triangleleft (d_j, c_j) \quad \text{if and only if} \quad \gamma_{i,c_i} > \gamma_{j,c_j} \quad (18)$$

where γ denotes the risk score of the particular classes of corresponding images. Considering this scenario, the posterior probability $p_{ij,c}$ of the image (d_i, c_i) is ranked higher than (d_j, c_j) is given by:

$$p_{ij,c} = \frac{e^{\gamma_{i,c_i} - \gamma_{j,c_j}}}{1 + e^{\gamma_{i,c_i} - \gamma_{j,c_j}}} \quad (19)$$

and the desired target value for the posterior probability is now given by:

$$\bar{p}_{ij,c} = 0.5 \times (1 + \hat{g}_{i,c_i} - \hat{g}_{j,c_j}), \quad (20)$$

where \hat{g}_{i,c_i} and $\hat{g}_{j,c_j} \in \{0, 1\}$ denote the risk labels of pairs. If a pair \hat{g}_{i,c_i} is mislabeled, $\hat{g}_{i,c_i} = 1$; otherwise, $\hat{g}_{i,c_i} = 0$. The objective is to minimize the difference between p_{ij} and \bar{p}_{ij} . The straightforward way to optimize the objective is to perform comparisons over all the images with various classes. However, this approach may be biased if certain classes have higher risk score and it does not account for the relative performance of each class.

Therefore, rather than using the individual-based approach, we present a voting-based mechanism for ranking images. For each item (d_i, c_i) , we count the number of wins, defined as the instances where (d_i, c_i) is ranked higher than (d_j, c_j) :

$$W_i = \sum_{d_i, c_i} \text{Indicator}(\gamma_{i,c_i} > \gamma_{j,c_j}) \quad (21)$$

here, $\text{Indicator}(\cdot)$ returns 1 if the condition is met and 0 otherwise. In case of a tie between class votes, our method resolves the ranking by prioritizing the pair with the highest aggregated risk score. This approach results in class-specific and balanced rankings for each image, prioritizing those with a higher number of risky classes. The example below further describes the process:

Example 4.4. *In a breast cancer classification task with four classes (benign, malignant, in situ, and invasive), consider two images, d_i and d_j , with predicted class probability vectors $d_i = [0.2, 0.6, 0.1, 0.1]$ and $d_j = [0.3, 0.4, 0.2, 0.1]$. Performing pairwise comparisons, d_i wins against d_j in the malignant class (1 win) but loses in the benign and in situ classes (0 wins each), while both images tie in the invasive class. The total win count results in $W_i = 1$ for d_i and $W_j = 2$ for d_j . Consequently, d_j is ranked higher due to its superior win count, demonstrating the effectiveness of the voting-based mechanism for class-based image ranking.*

If (d_i, c_i) is mislabeled and (d_j, c_j) is correctly labeled, the optimization process will maximize $\gamma_{i,c_i} - \gamma_{j,c_j}$ for all the class using the aggregated p_{ij} and \bar{p}_{ij} scores in a multiclass scenario, the cross-entropy loss function is extended to account for multi-class pairs as follows:

$$L(D_\gamma) = \sum_{(d_i, c_i), (d_j, c_j) \in D_\gamma} -\bar{p}_{ij} \log(p_{ij}) - (1 - \bar{p}_{ij}) \log(1 - p_{ij}), \quad (22)$$

in which the value of $L(D_\gamma)$ increases with the value difference between p_{ij} and \bar{p}_{ij} as desired.

We also introduced dropout during training to randomly set a percentage of input units to zero. This prevents co-adaptation and promotes the learning of more robust features for each class. Dropout is inactive during evaluation, with activations scaled for consistency. In multiclass classification, dropout helps prevent overfitting by ensuring that the model does not overly rely on specific features. We set the dropout rate to 0.5 and fine-tuned it for optimal performance.

5. Solution for MultiRisk Based Adaptive Training

Neural networks using softmax for multiclass tasks often produce overly confident predictions, which can mislead training and impair generalization [13]. Class imbalance can further degrade performance on minority classes [20], and risk estimation may fail to accurately reflect misclassification likelihood, particularly in complex multiclass scenarios [19].

Our solution, detailed in Algorithm 3 and Figure 1, involves two phases: traditional pre-training and risk-based adaptive training.

- **Traditional Pre-Training Phase:** During this initial phase, a deep model undergoes training using conventional methods, relying on labeled training data. In our method, we use four CNN deep models and train all of them on the given workload with arguably the best parameters. The aim is to try to achieve the best test efficacy for each model.
- **Risk Based Adaptive Training Phase:** This phase aims to enhance model performance by focusing on high-risk instances and managing prediction uncertainties. This framework integrates temperature scaling to reduce overconfidence and Value at Risk (VaR) to assess misclassification risks. The goal is to improve the robustness and accuracy of the classifier. The step-wise process is given below:

Algorithm 3 Risk-Based Adaptive Training for Multiclass Breast Cancer Detection

Input: A workload of Multiclass Breast Cancer histopathological images D consisting of D_s , D_v , D_t and initial classifier $g(\omega)$;

Output: A learned classifier $g(\omega_*)$;

- 1: $\omega_0 \leftarrow$ Initialize ω with random values;
 - 2: **for** $k = 0$ to $m - 1$ **do**
 - 3: Train the classifier using the standard cross-entropy loss on the training set D_s :
 - 4: $\omega_{(k+1)} \leftarrow \omega_{(k)} - \alpha \nabla_{\omega_k} L_{\text{train}}(\omega_k)$;
 - 5: **end for**
 - 6: Select the best model $g(\omega_*)$ based on validation set D_v ;
 - 7: $\omega_m \leftarrow \omega_*$;
 - 8: Train the risk model using the validation set D_v :
 - 9: **for** each instance $i \in D_v$ **do**
 - 10: Calculate $\text{VaR}_\theta(i)$ for each class;
 - 11: **end for**
 - 12: **for** $k = m$ to $m + n - 1$ **do**
 - 13: Update the model using the test set D_t with labels predicted by the risk model:
 - 14: **for** each instance $i \in D_t$ **do**
 - 15: Predict the probabilities P_{original} for each class;
 - 16: Regularize the predictions:
 - 17: $P_{\text{regularized}}(i) = \frac{\exp(z_i/\lambda)}{\sum_{j=1}^C \exp(z_j/\lambda)}$;
 - 18: Compute the cross-entropy loss L using $P_{\text{regularized}}$ and true labels;
 - 19: **end for**
 - 20: Update the model parameters:
 - 21: $\omega_{(k+1)} \leftarrow \omega_{(k)} - \alpha \nabla_{\omega_k} L(\omega_k)$;
 - 22: Recalculate the risk values and update λ ;
 - 23: **end for**
 - 24: Select the last trained model $g(\omega_*) \leftarrow g(\omega_{(k+1)})$;
 - 25: **return** $g(\omega_*)$;
-

In the second phase, the algorithm first uses the validation set D_v to train the risk model, focusing on estimating the Value at Risk (VaR) for each instance to aid in risk assessment. This involves identifying high-risk instances through VaR calculations for additional training or correction. Then, it ap-

plies the trained risk model to predict labels for the test set D_{test} , assigning tentative labels based on the lowest risk as indicated by VaR. Finally, it fine-tunes the classifier using the instances in D_{test} and their predicted labels, with the goal of minimizing misclassification risk as guided by VaR.

Observing that models relying on softmax outputs often produce overconfident predictions, we propose to smooth the predicted probability distribution for improved calibration. Guo et al. [34] highlighted that techniques like temperature scaling can enhance calibration without complex calculations. By applying logits scaling with a custom softmax activation function that incorporates a learnable temperature parameter λ , we adaptively scale the logits, as shown in equation 23, as follows:

$$P_{\text{regularized}}(i) = \frac{\exp(z_i/\lambda)}{\sum_{j=1}^C \exp(z_j/\lambda)}, \quad (23)$$

where the parameter λ is initialized at 2 and updated during training to balance regularization. Here, z_i represents the logits for class i , C is the total number of classes, and \exp denotes the exponential function. We use cross-entropy loss to calculate the difference between predictions and true targets, while the SGD optimizer adjusts λ based on gradients from back-propagation. Iterative updates in the training loop minimize the loss, ensuring effective learning, the process is represented as:

$$L(Y, P_{\text{regularized}}, \lambda) = -\frac{1}{N} \sum_{i=1}^N Y_i \log(P_{\text{regularized}}(i)) \quad (24)$$

where L is the Cross Entropy Loss applied to the adjusted probabilities $P_{\text{regularized}}$. Y_i is the one-hot encoded true label for the i -th sample, N is the total number of samples in the batch, and \log is the natural logarithm. The parameter λ regulates the temperature of the softmax probabilities, improving regularization, and is iteratively updated during training using gradients.

6. Empirical Study

This section evaluates the performance of our proposed approach by an empirical study. It is organized as follows: Subsection. 6.1 describes experimental setup; Subsection. 6.2 presents the evaluation results of risk analysis; Subsection. 6.3 presents the evaluation results of adaptive learning; Subsection. 6.4 presents the evaluation results of sensitivity study; finally, Subsection. 6.5 presents the evaluation results of ablation study.

6.1. Experimental Setup

Table 4: The statistics of the BRACS dataset

	N	PB	UDH	FPA	ADH	DCIS	IC	Total
Train	357	714	389	624	387	665	521	3657
Validation	46	43	46	49	41	40	47	312
Test	81	79	82	83	79	85	81	570

Table 5: The statistics of the BACH Dataset

Dataset	Normal	Benign	DCIS	IC	Total
Train	357	650	665	521	2193
Validation	16	16	16	16	64
Test	20	20	20	20	80

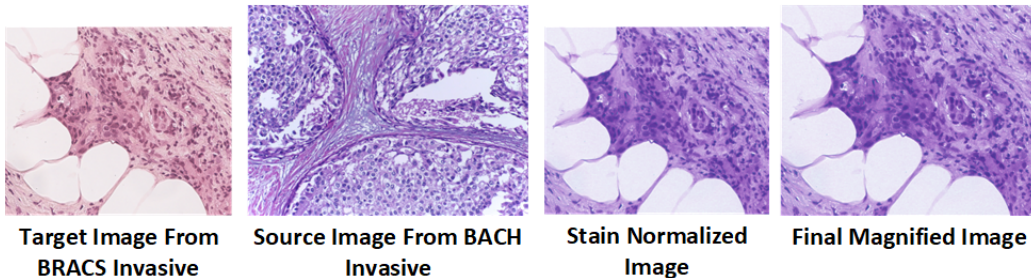


Figure 3: Stain Normalization on BRACS

We have used two open-sourced benchmark datasets of real H&E stained histopathological breast cancer images, BRACS [6] and BACH. They can be briefly described as follows:

- **BRACS.** The BReAst Carcinoma Subtyping (BRACS) dataset is a large, annotated collection of 547 Whole-Slide Images (WSIs) and 4539 Regions Of Interest (ROIs) from over 150 patients, aimed at advancing AI for breast cancer characterization. Annotated by three pathologists, the dataset categorizes lesions into three categories and seven subtypes, making it the most comprehensive dataset available for breast cancer subtyping. Table 4 shows the statistics of this dataset.

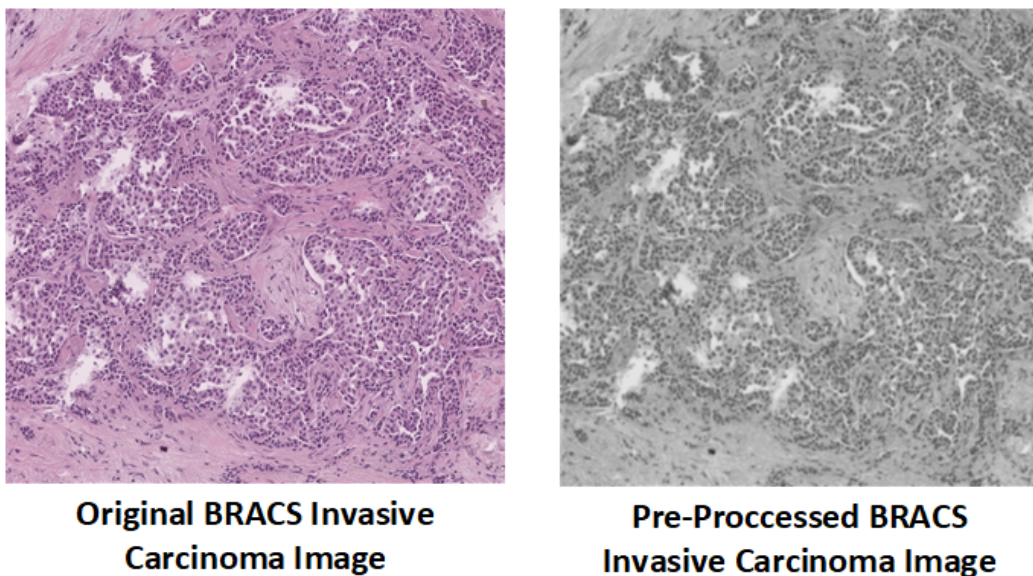


Figure 4: Sample for Original image and Low-Resolution Image from Invasive Carcinoma Class of BRACS

- **BACH.** The BACH dataset from the ICIAR 2018 grand challenge contains 400 ROI microscopy images, 100 for each of its four classes. Due to its limited size, we combined BACH with the BRACS dataset, as both share similar image types. For adaptive learning evaluation, we used BRACS for training and BACH for validation and testing. Table 5 shows the statistics of this dataset.

Additionally, we have converted the original BRACS dataset to a low-resolution version, creating a third dataset, as CNNs and Transformers perform better on low-resolution images. Our experiments have been conducted on the original BRACS with varying image sizes, low-resolution BRACS, and the BRACS-BACH datasets.

For the evaluation of cross-domain risk analysis and adaptive learning, we used the BRACS and BACH [3] breast histopathological datasets. We combined them into a new four-class dataset (Normal, Benign, In Situ, and Invasive), merging BRACS’s benign and hyperplasia classes into one. Macenko stain normalization [17] addressed staining differences, and BRACS images were resized to 20x magnification for uniformity. The dataset was balanced by selecting proportionate images from each class. For the seven-

class task, we used both the original and a low-resolution grayscale BRACS dataset at 512 x 512 pixels. Figure 3 and 4 shows a sample of preprocessing on given images.

For misprediction risk analysis, we train several state-of-the-art models, including Densenet121, Densenet201, Resnet50, EfficientnetB4, and the transformer-based CCT; then, we choose the top-performing model as the classifier baseline, while using the others to generate diverse risk features. All the models were trained for 200 epochs while for Resnet50, Densenet121, Densenet201 and CCT, the initial learning rate was set to 0.0005 and for EfficientnetB4, the learning rate was set to 0.001. Furthermore, SGD optimizer and Cross Entropy loss function were employed to optimize the performance of the models. The Learning rate for risk model training was set between the range from 0.0005 to 0.00005.

For misprediction risk analysis, we compare the proposed approach, denoted by MultiRisk with the following alternatives:

- **Baseline** [16]: This technique evaluates uncertainty by focusing on the classifier’s output probability. Predictions near 1 indicate confidence, while those closer to 0 imply uncertainty. The uncertainty score is calculated as $1 - P(e_{ij}|m_i)$, emphasizing uncertainty over confidence.
- **TrustScore** [19]: TrustScore calculates a score based on the agreement between the classifier and a nearest-neighbor classifier using features from DCA’s layer. We use the official implementation with default settings.
- **ConfidNet** [10]:ConfidNet adds a confidence scoring module to the main network. This 5-layer module with ReLU activations computes the confidence score, trained using the True Class Probability (TCP) criterion.
- **LearnRisk** [8]: This approach implements the straightforward Learn-Risk solution for multi-class classification, constructing a separate risk model for each class.

For the evaluation of risk-based adaptive learning, we compare our solution with state-of-the-art deep models and approaches for multiclass breast cancer detection, which are described as follows:

- **HactNet [33]:** HactNet creates Hierarchical Cell-to-Tissue (HACT) graph representations for classifying ROI images and compares results with pathologists’ predictions.
- **ScoreNet [40]:** ScoreNet is a Transformer-based method that uses scoremix augmentation to achieve top classification performance on BRACS ROIs, comparing favorably with various techniques, including multiple instance learning and GNNs.
- **TransPath [44]:** A Transformer-based model for histopathological image classification that utilizes attention mechanisms to effectively capture complex patterns and relationships in image data.
- **CTransPath [45]:** The study presents Semantically-Relevant Contrastive Learning (SRCL) to enhance self-supervised learning in medical image analysis by employing a hybrid CTransPath model that combines CNN and Swin Transformer for improved histopathological image tasks.
- **SCDA [24]:** SCDA (Semantic Concentration for Domain Adaptation) focuses on key features through pair-wise adversarial alignment of prediction distributions, unlike typical distribution alignment methods. This approach is used for domain transfer evaluation.
- **TSA [23]:** TSA (Transferable Semantic Augmentation) improves classifier adaptation by augmenting source features with random directions from a multivariate normal distribution to reflect semantic changes in the input space, and is applied for domain transfer evaluation.
- **CNNs:** We also compared our approach with multiple CNNs used to get features for the MultiRisk Approach.
- **CCT [27]:** The Compact Convolutional Transformer (CCT) merges the strengths of CNNs and transformers, achieving top performance in tasks such as image classification, object detection, and semantic segmentation.
- **Ensemble:** Ensemble learning for all the CNNs and CCT used to generate risk features for the MultiRisk approach.

- **LearnRisk** [8]: Uses a Risk Model for misprediction risk analysis and adaptive training to enhance the performance of state-of-the-art approaches.

As usual, for the evaluation of risk analysis, we use the metric of AUROC; for the evaluation of adaptive learning, we use the metrics of accuracy, precision, recall, F1 and classwise F1.

6.2. Evaluation Results of Risk Analysis

Figure 5 presents the detailed comparative results for AUROC analysis of MultiRisk with SOTA methods. It can be observed that on the original BRACS dataset, the AUROC of the Baseline stands at 73% and the LearnRisk with 74.6%, while ConfidNet, and TrustScore fails to surpass the Baseline’s performance. Remarkably, MultiRisk demonstrates considerable improvement with an AUROC of 78.1%, marking a noteworthy enhancement of 5.1% compared to the Baseline. The results on the BRACS(512 x 512) dataset are similar. The Baseline records an AUROC of 72.9% and LearnRisk with 73.8%, with ConfidNet, and TrustScore falling short of outperforming the Baseline in the multiclass setting. Once again, MultiRisk showcases its effectiveness by achieving an AUROC of 75.6%, with an improvement of 2.7% over the Baseline. These results underscore the efficacy of the MultiRisk approach in enhancing risk analysis performance.

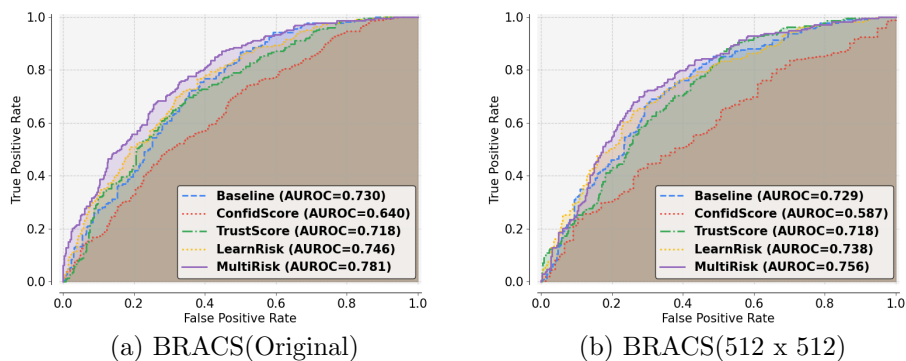


Figure 5: Performance of Risk Analysis on Original and Low Resolution BRACS Respectively

To further evaluate the efficacy of MultiRisk, we have also conducted a domain transfer evaluation, where we used the BRACS-BACH four-class

dataset. In this experiment, the baseline classifier was trained on BRACS samples but risk model was trained on BACH samples. The detailed evaluation results have been presented in Figure 6. It can be observed that MultiRisk achieved an AUROC of 76.3%, a 2.4% improvement over the Baseline’s 73.9%. While LearnRisk reached 74.3%, both ConfidNet and TrustScore failed to outperform the Baseline. These results highlight MultiRisk’s effectiveness in enhancing risk assessment models in the scenario of domain transfer.

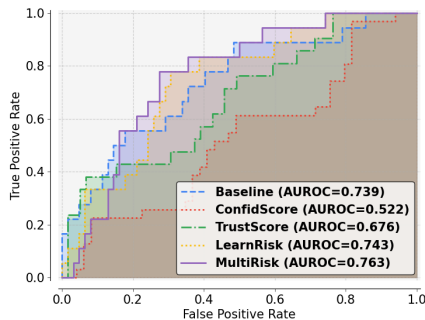


Figure 6: AUROC Evaluation for BRACS-BACH Domain Transfer Task

6.3. Evaluation Results of Risk-based Adaptive Learning

Table 6: The comparative evaluation results of adaptive learning on original BRACS images

Method	Accuracy (%)	F1 (%)	Precision (%)	Recall (%)	AUC (%)
Densenet121	60.70	60.65	61.08	60.70	90.84
Resnet50	56.67	55.88	56.20	56.67	87.30
Efficientnet B4	60.53	59.39	58.76	60.53	88.29
CCT	54.39	53.97	55.45	54.39	87.19
Ensemble	59.12	58.36	58.02	59.12	89.63
TransPath	56.27	55.1	55.41	56.27	86.1
CTransPath	57.36	56.75	56.07	57.36	87.14
LearnRisk	62.11	60.05	60.93	61.81	89.30
MultiRisk(Ours)	63.51	61.15	61.80	63.51	91.38

We have presented the detailed comparative results in Table 6 and 7. As shown in Table 6, on the original BRACS dataset, MultiRisk outperforms four deep learning models, including ensemble approach and high-performing architectures like TransPath, CTransPath, and LearnRisk, on

all the performance metrics. By enhancing multiclass prediction accuracy through misprediction risk analysis based on the baseline Densenet121, MultiRisk demonstrates robustness and adaptability across datasets.

As shown in Table 7, on the BRACS(512 x 512) dataset, MultiRisk similarly outperforms with 66.34% accuracy, with a 3.01% improvement over the baseline. It also achieves improved performance in terms of F1-score, precision, recall, and AUC, by the margins of 2.57%, 1.72%, 3.01%, and 1.34% respectively. While TransPath and CTransPath had comparable results, MultiRisk consistently secured the highest metrics, highlighting its robustness and efficacy across the different image resolutions.

Table 7: The comparative evaluation results of adaptive learning on BRACS(512 x 512) images

Method	Accuracy (%)	F1 (%)	Precision (%)	Recall (%)	AUC (%)
Densenet121	63.33	63.41	64.51	63.33	90.73
Resnet50	63.33	62.88	64.56	63.33	89.64
Densenet201	63.16	62.97	63.37	63.16	89.98
CCT	60.70	60.27	60.85	60.70	89.13
Ensemble	62.63	62.70	63.32	62.63	90.74
TransPath	58.17	57.1	57.52	58.17	87.23
CTransPath	60.17	59.7	59.02	60.17	88.7
LearnRisk	65.09	64.23	64.40	64.93	90.10
MultiRisk(Ours)	66.34	65.98	66.23	66.34	92.07

We have also presented the comparative evaluation results of classwise F1-score and weighted F1-score in Table 8. It can be observed that MultiRisk achieves an impressive weighted F1 score of 65.98, surpassing the previous leading transformer-based approach, ScoreNet. Although ScoreNet excels in the flat epithelial atypia class, classical models such as Densenet121, Densenet201, and Resnet50 outperform it in Atypical Ductal Hyperplasia, Usual Ductal Hyperplasia, and Ductal Carcinoma in situ. Notably, MultiRisk improves the F1 score for 6 out of 7 classes in the multiclass setting, demonstrating superior performance in the normal, pathological benign, and Invasive Carcinoma classes compared to the baseline. Specifically, it shows a 6.2% improvement in normal ductal hyperplasia, and 4.41% in flat epithelial atypia. For cancer classes, MultiRisk achieves notable enhancements of 1.6% for ductal carcinoma in situ and 6.73% for invasive carcinoma.

Despite not surpassing SOTA models in the Atypical Ductal Hyperplasia class, this can be attributed to the overall underperformance of non-baseline

models in that category. HactNet is widely regarded as the most reliable approach for the BRACS dataset, validated against assessments by real-world pathologists. Notably, MultiRisk outperforms HactNet in nearly every class, achieving an overall improvement of 4.48% in the weighted F1 score.

Table 8: Mean and Standard Deviation evaluation for each class F1 and weighted F1 score using state-of-the-art methods

Method	0_N	1_PB	2_UDH	3_FEA	4_ADH	5_DCIS	6_IC	Weighted F1
Densenet121	77.01±4.5	52.9±2.6	42.2±1.9	73.5±3.5	50.9±2.5	62.06±3.1	84.5±3.5	63.41±1.5
Densenet201	77.83±3.9	52.3±2.3	57.6±2.7	69.2±3.3	44.7±2.0	58.46±4.2	80.7±3.6	62.97±3.1
Resnet50	76.5±3.7	46.3±2.5	52.1±2.6	74.6±3.5	36.5±1.6	66.6±3.2	85.8±3.7	62.88±1.4
CCT	73±4.1	40.6±2.2	50±2.4	75.2±3.5	37.2±1.7	58.7±2.8	85.5±3.6	60.27±1.7
Ensemble	75.77±3.3	47.72±3.0	49.16±1.8	77.84±2.8	39.13±1.8	60.86±2.7	87.34±3.1	62.70±1.9
TransPath	58.8±2.7	43.4±2.3	35.2±4.3	67.2±6.1	38.6±1.8	61.7±1.4	85.4±1.6	57.1±2.1
CTransPath	60.0±1.4	47.1±2.7	37.9±2.3	72.9±3.1	43.3±3.8	65.9±1.4	91.0±2.6	59.7±1.1
HACT-Net	61.6±2.1	47.5±2.9	43.6±1.9	74.2±1.4	40.4±2.5	66.4±2.6	88.4±0.2	61.5±0.9
ScoreNet	64.3±1.5	54.0±2.2	45.3±3.4	78.1±2.8	46.7±1.0	62.9±2.0	91.0±1.4	64.4±0.9
LearnRisk	77.71±4.4	53.98±2.6	46.97±2.1	76.92±3.1	44.11±2.6	61.45±1.8	88.46±1.3	64.23±0.9
MultiRisk(Ours)	78.30±4.3	54.71±2.6	48.40±2.3	77.91±3.9	47.62±2.1	63.66±2.1	91.23±2.7	65.98±1.0

To further validate the efficacy of MultiRisk, we have also conducted an empirical study on the domain-transfer BRACS-BACH dataset where training images come from BRACS but validation and test images come from BACH. Besides the existing leading deep models, we also compare MultiRisk with an ensemble of these models, LearnRisk and two SOTA domain transfer learning approaches, SCDA and TSA.

Table 9: Accuracy, F1-Score, Precision, Recall, and AUC Evaluation for BRACS-BACH Domain Transfer Task

Model	Accuracy (%)	Precision (%)	Recall (%)	AUC (%)
Efficientnet_B4	77.50	79.08	77.50	92.35
Densenet121	73.75	74.17	73.75	88.58
CCT	70.00	71.35	70.00	89.38
Resnet50	67.50	67.93	67.50	87.65
Ensemble	70.00	72.65	70.00	89.54
SCDA	78.91	79.45	78.91	89.74
TSA	72.64	72.94	72.64	86.76
LearnRisk	77.50	79.25	77.50	92.93
MultiRisk(Ours)	80.00	81.90	80.00	93.23

We have presented the overall comparative evaluation results in Table 9. It can be observed that MultiRisk outperforms its alternatives on all the met-

Table 10: F1 Score Evaluation for BRACS BACH Domain Transfer Task

Model	Normal	Benign	InSitu	Invasive	Weighted F1
EfficientnetB4	86.48±4.2	60.46±3.5	78.04±4.3	87.17±4.5	78.04±1.0
Resnet50	72.34±4.5	29.41±2.4	69.76±4.0	77.77±3.5	67.33±1.9
Densenet121	78.04±4.2	55.00±3.0	80.95±4.4	81.08±3.4	73.77±1.0
CCT	87.17±4.5	47.36±3.1	65.21±4.4	81.08±3.5	70.21±1.5
Ensemble	86.48±±4.2	51.16±3.2	68.18±4.0	83.33±3.5	70.84±1.5
SCDA	86.51±±4.2	60.63±3.3	80.50±4.1	87.12±±3.9	78.69±1.0
TSA	86.45±3.1	65.92±3.9	71.05±2.6	70.64±4.7	72.01±1.3
LearnRisk	83.33±4.1	60.46±3.5	80.95±4.3	87.17±4.5	77.98±1.0
MultiRisk(Ours)	88.88±4.1	65.11±3.5	80.95±4.3	87.17±4.5	80.53±0.9

rics, underscoring its efficacy in domain-transfer scenarios. We have also presented the detailed class-wise F1 scores in Table 10. It can be observed that MultiRisk outperforms the baseline (EfficientNet-B4), with improvements of 2.4% for Normal, 4.64% for Benign, and 2.9% for InSitu, while showing no considerable change for Invasive. Although SCDA also outperforms the deep models and even LearnRisk, TSA shows limited efficacy compared with them, because ideally TSA was built for large amount of data from all the domains, and in this scenario due to the limited number of validation and test images compared to the cross-domain training images its efficacy is limited.

We have also visualized the comparative results by confusion matrix as shown in Figure 7. In Figure 7 (a), it can be observed that MultiRisk correctly classifies 364 of 570 test images on the original BRACS dataset, achieving the highest accuracy in "Invasive Carcinoma" (75/81), while mispredictions mainly occurred between "Pathological Benign," "Usual Ductal Hyperplasia," and "Atypical Ductal Hyperplasia." In Figure 7 (b), for the BRACS(512 x 512) dataset, MultiRisk accurately predicts 375 of 512 images, with similar errors in distinguishing between "Pathological Benign," "Usual Ductal Hyperplasia," and "Atypical Ductal Hyperplasia." Finally, for the domain transfer analysis, the confusion matrix in Figure 7 (c) shows that, using 80 test images from BRACS-BACH, MultiRisk accurately classifies 64 images, with mispredictions mainly between "Normal" and "Benign" classes, highlighting both strengths and areas for improvement in class differentiation and domain transfer.

Finally, to analyze the qualitative performance of MultiRisk-based adaptive training, we showcase a qualitative analysis of ROI images across all

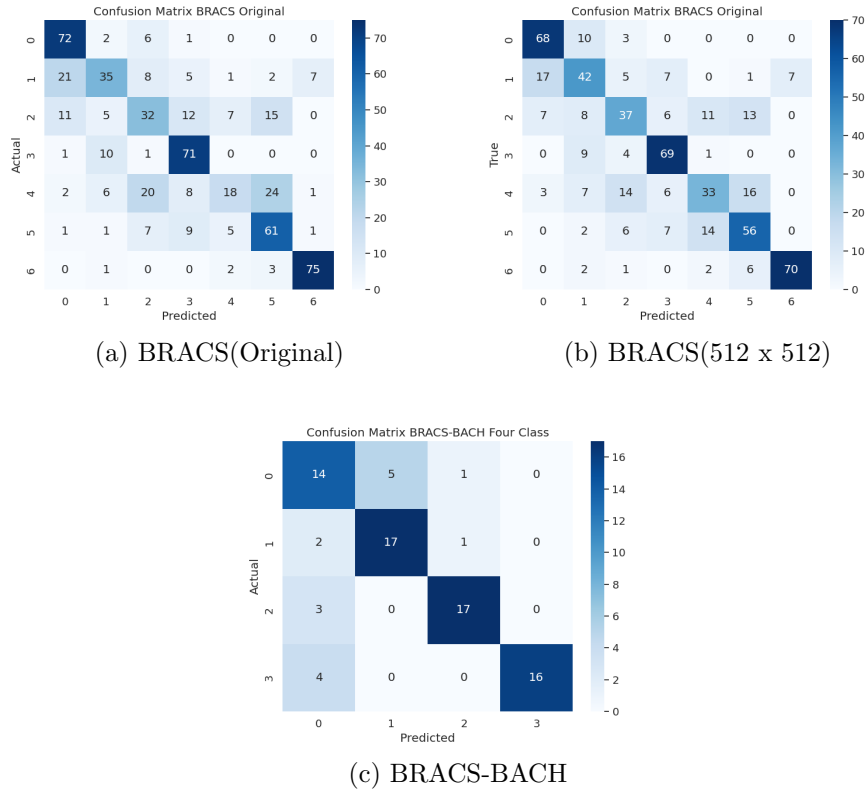


Figure 7: Confusion Matrix Analysis of MultiRisk for all three datasets

three datasets using GradCam [38], which generates heatmaps of class activations, in Figure 8. The results indicate that MultiRisk not only corrects mispredictions for all classes but also identifies additional tumor regions. Notable corrections include transitions from ADH to DCIS, DCIS to IC in the original BRACS dataset, N to IC in BRACS(512x512), and Benign to InSitu during the domain transfer task.

6.4. Sensitivity Study of Risk Analysis

In the sensitivity study, we have evaluated the sensitivity of risk model w.r.t validation samples by conducting two experiments, the first experiment using a different number of validation samples, and the second one using the same number but randomly selected validation samples. Note that the training and test samples remain the same in the sensitivity study. Additionally, we have also evaluated the efficacy of MultiRisk by leveraging different

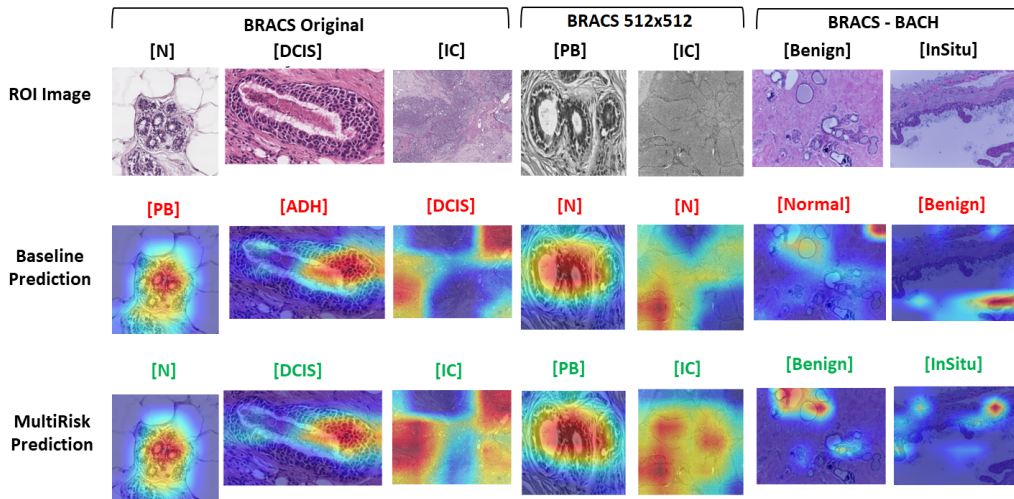


Figure 8: Qualitative Comparison between Baseline and MultiRisk, class labels and predictions, where red denotes misprediction and green denotes correctly predicted

baseline classifier models.

The evaluation results w.r.t the number of validation samples have been presented in Figure 9 (a), (b) and (c). The evaluation results w.r.t random validation samples have been presented in Figure 9 (d), (e) and (f). It can be observed that in both cases, the performance of MultiRisk is robust across all three datasets. A nominal change under 1% is recorded while performing these experiment across all three datasets.

Furthermore, the evaluation results on the performance sensitivity of MultiRisk-based adaptive learning with different Baseline models have been presented in Table 11. It can be observed that on each baseline model, MultiRisk outperforms both the baseline and LearnRisk. These results clearly demonstrate the performance robustness of the MultiRisk-based approach.

6.5. Ablation Study

To validate the design choices made in MultiRisk and MultiRisk-based adaptive learning, we have conducted an ablation study, in which we remove certain new mechanisms during each major step and compare the performance of combined MultiRisk Mechanism with selected original LearnRisk based mechanisms.

The detailed evaluation results in terms of ROC have been presented in Table 12. It can be observed that MultiRisk achieves the overall highest

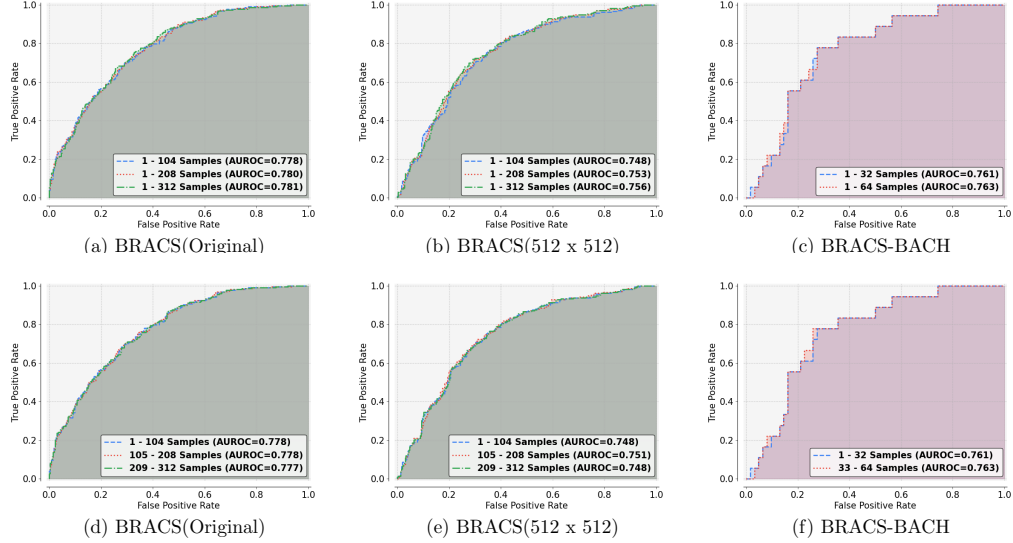


Figure 9: Sensitivity Analysis of MultiRisk for all three datasets, Validation Samples with Different number and type of samples varying from 104 to 312, and 0, 312

performance at 78.1%, and 76.3% on the original BRACS, and BRACS-BACH datasets respectively, while a nominal difference was recorded for BRACS(512x512) dataset where MultiRisk still performs the second best. The evaluation results in terms of accuracy and F1 have also been shown in Table 12. In most cases, MultiRisk outperforms other methods, although for the domain transfer task, accuracy and F1 scores are often similar due to the fewer validation and test images compared to training images.

Table 11: Performance Comparison of MultiRisk Based on Different Baselines

Model	Baseline		LearnRisk		MultiRisk	
	Accuracy	F1	Accuracy	F1	Accuracy	F1
Resnet50	63.33	62.88	64.21	63.40	65.04	64.08
EfficientNetB4	58.25	56.74	58.95	56.36	59.47	57.03
CCT	60.7	60.27	61.58	60.27	62.90	61.97
Densenet201	63.16	62.97	63.33	63.03	63.41	63.1
Densenet121	63.33	63.44	65.09	64.23	66.34	65.98

Table 12: Comparison of Methods on Different Datasets where each time we run the approach excluding one step from our method and including the method from LearnRisk

Method	Dataset	Accuracy	F1 Score	Risk AUROC
Risk Feature Generation (LearnRisk)	BRACS(Original)	59.65 ± 2.0	58.44 ± 1.8	73.2
	BRACS(512 x 512)	63.86 ± 3.8	63.41 ± 2.4	75.3
	BRACS-BACH	75.00 ± 12.1	75.63 ± 10.3	67.8
Risk Model Construction/Training (LearnRisk)	BRACS(Original)	62.81 ± 1.2	61.20 ± 1.7	78.1
	BRACS(512 x 512)	65.07 ± 3.7	64.23 ± 4.9	76.2
	BRACS-BACH	75.00 ± 9.3	75.63 ± 10.3	72.0
Risk Based Adaptive Training (LearnRisk)	BRACS(Original)	61.40 ± 4.3	59.43 ± 5.1	73.5
	BRACS(512 x 512)	63.86 ± 1.3	62.87 ± 2.7	75.3
	BRACS-BACH	80.00 ± 1.4	80.53 ± 1.1	69.8
MultiRisk (Ours)	BRACS(Original)	63.51 ± 2.0	61.15 ± 1.4	78.1
	BRACS(512 x 512)	66.34 ± 2.3	65.98 ± 1.0	75.6
	BRACS-BACH	80.00 ± 1.3	80.53 ± 0.9	76.3

7. Conclusion and Future Work

In this paper, we have proposed a novel approach to misprediction risk analysis, **MultiRisk**, for multiclass breast cancer detection. MultiRisk introduces new mechanisms for risk feature generation, risk model construction and training, and risk-based adaptive training, which are specifically designed for multiclass problems and effectively enable accurate misprediction quantification. Based on the MultiRisk approach, we have also presented an adaptive learning solution that can efficiently fine-tune a baseline multiclass model to a target workload. Our extensive experiments on real benchmark datasets validate the efficacy of the proposed solutions.

For future work, it is noteworthy that the proposed **MultiRisk** approach is potentially applicable to other types of cancer detection; however, its technical details require further investigation. Additionally, the current solution extracts risk metrics based on mainstream deep neural network (DNN) models, which have limited overall interpretability. To enhance both the **efficacy** and **interpretability** of risk analysis, future research could explore generating risk features using explainable AI techniques.

Author Contributions

Gul Sheeraz led the study, handled data curation, formal analysis, investigation, methodology development, project administration, and drafting. Qun Chen provided funding, resources, supervision, and manuscript review. Liu Feiyu contributed to analysis, investigation, methodology, software, validation, visualization, and manuscript review. Zhou Fengjin provided supervision related to medical information for this task.

Declaration of Generative AI and AI-assisted technologies in the writing process

The authors used ChatGPT 4.0 to enhance writing flow in some sections. They reviewed and edited the content afterward, taking full responsibility for the final manuscript.

Acknowledgments

This work is supported by the National Key Research and Development Program of China under the project number 2023YFB4503600, and National Natural Science Foundation of China under Grant No. 62172335.

References

- [1] Alzubaidi, L., Al-Amidie, M., Al-Asadi, A., Humaidi, A.J., Al-Shamma, O., Fadhel, M.A., Zhang, J., Santamaría, J., Duan, Y., 2021. Novel transfer learning approach for medical imaging with limited labeled data. *Cancers* 13, 1590.
- [2] Araújo, T., Aresta, G., Castro, E., Rouco, J., Aguiar, P., Eloy, C., Polónia, A., Campilho, A., 2017. Classification of breast cancer histology images using convolutional neural networks. *PloS one* 12, e0177544.
- [3] Aresta, G., Araújo, T., Kwok, S., Chennamsetty, S.S., Safwan, M., Alex, V., Marami, B., Prastawa, M., Chan, M., Donovan, M., et al., 2019. Bach: Grand challenge on breast cancer histology images. *Medical image analysis* 56, 122–139.
- [4] Arya, N., Saha, S., 2021. Multi-modal advanced deep learning architectures for breast cancer survival prediction. *Knowledge-Based Systems* 221, 106965.
- [5] Bejnordi, B.E., Veta, M., Van Diest, P.J., Van Ginneken, B., Karssemeijer, N., Litjens, G., Van Der Laak, J.A., Hermsen, M., Manson, Q.F., Balkenhol, M., et al., 2017. Diagnostic assessment of deep learning algorithms for detection of lymph node metastases in women with breast cancer. *Jama* 318, 2199–2210.
- [6] Brancati, N., Anniciello, A.M., Pati, P., Riccio, D., Scognamiglio, G., Jaume, G., De Pietro, G., Di Bonito, M., Foncubierta, A., Botti, G., et al., 2022. Bracs: A dataset for breast carcinoma subtyping in h&e histology images. *Database* 2022, baac093.

- [7] Brown, G., Pocock, A., Zhao, M.J., Luján, M., 2012. Conditional likelihood maximisation: a unifying framework for information theoretic feature selection. *The journal of machine learning research* 13, 27–66.
- [8] Chen, Z., Chen, Q., Hou, B., Li, Z., Li, G., 2020. Towards interpretable and learnable risk analysis for entity resolution, in: *Proceedings of the 2020 ACM SIGMOD international conference on Management of data*, pp. 1165–1180.
- [9] Ciga, O., Xu, T., Martel, A.L., 2022. Self supervised contrastive learning for digital histopathology. *Machine Learning with Applications* 7, 100198.
- [10] Corbière, C., Thome, N., Bar-Hen, A., Cord, M., Pérez, P., 2019. Addressing failure prediction by learning model confidence. *Advances in Neural Information Processing Systems* 32.
- [11] Elfgen, C., Papassotiropoulos, B., Varga, Z., Moskovszky, L., Nap, M., Güth, U., Baege, A., Amann, E., Chiesa, F., Tausch, C., 2019. Comparative analysis of confocal microscopy on fresh breast core needle biopsies and conventional histology. *Diagnostic pathology* 14, 1–8.
- [12] Guida, F., Kidman, R., Ferlay, J., Schüz, J., Soerjomataram, I., Kithaka, B., Ginsburg, O., Mailhot Vega, R.B., Galukande, M., Parham, G., et al., 2022. Global and regional estimates of orphans attributed to maternal cancer mortality in 2020. *Nature medicine* 28, 2563–2572.
- [13] Guo, C., Pleiss, G., Sun, Y., Weinberger, K.Q., 2017. On calibration of modern neural networks, in: *International conference on machine learning*, PMLR. pp. 1321–1330.
- [14] Guo, W., Wang, J., Wang, S., 2019. Deep multimodal representation learning: A survey. *Ieee Access* 7, 63373–63394.
- [15] Guyon, I., Weston, J., Barnhill, S., Vapnik, V., 2002. Gene selection for cancer classification using support vector machines. *Machine learning* 46, 389–422.
- [16] Hendrycks, D., Gimpel, K., 2016. A baseline for detecting misclassified and out-of-distribution examples in neural networks. *arXiv preprint arXiv:1610.02136* .

- [17] Hoque, M.Z., Keskinarkaus, A., Nyberg, P., Seppänen, T., 2023. Stain normalization methods for histopathology image analysis: A comprehensive review and experimental comparison. *Information Fusion* , 101997.
- [18] Ji, J., Wan, T., Chen, D., Wang, H., Zheng, M., Qin, Z., 2022. A deep learning method for automatic evaluation of diagnostic information from multi-stained histopathological images. *Knowledge-Based Systems* 256, 109820.
- [19] Jiang, H., Kim, B., Guan, M., Gupta, M., 2018. To trust or not to trust a classifier. *Advances in neural information processing systems* 31.
- [20] Johnson, J.M., Khoshgoftaar, T.M., 2019. Survey on deep learning with class imbalance. *Journal of big data* 6, 1–54.
- [21] Jorion, P., 1997. Value at risk: the new benchmark for controlling market risk. (No Title) .
- [22] Li, L., Pan, H., Liang, Y., Shao, M., Xie, S., Lu, S., Liao, S., 2024. Pmfnn-ssl: Self-supervised learning-based progressive multimodal fusion network for cancer diagnosis and prognosis. *Knowledge-Based Systems* 289, 111502.
- [23] Li, S., Xie, M., Gong, K., Liu, C.H., Wang, Y., Li, W., 2021a. Transferable semantic augmentation for domain adaptation, in: *Proceedings of the IEEE/CVF conference on computer vision and pattern recognition*, pp. 11516–11525.
- [24] Li, S., Xie, M., Lv, F., Liu, C.H., Liang, J., Qin, C., Li, W., 2021b. Semantic concentration for domain adaptation, in: *Proceedings of the IEEE/CVF international conference on computer vision*, pp. 9102–9111.
- [25] Liang, Y., Meng, Z., 2023. Brea-net: An interpretable dual-attention network for imbalanced breast cancer classification. *IEEE Access* .
- [26] Luong, M.T., Pham, H., Manning, C.D., 2015. Effective approaches to attention-based neural machine translation. *arXiv preprint arXiv:1508.04025* .
- [27] Marefat, A., Marefat, M., Hassannataj Joloudari, J., Nematollahi, M.A., Lashgari, R., 2023. Cctcovid: Covid-19 detection from chest x-ray

- images using compact convolutional transformers. *Frontiers in Public Health* 11, 1025746.
- [28] Mehra, R., et al., 2018. Breast cancer histology images classification: Training from scratch or transfer learning? *ICT Express* 4, 247–254.
- [29] Nafa, Y., Chen, Q., Chen, Z., Lu, X., He, H., Duan, T., Li, Z., 2022. Active deep learning on entity resolution by risk sampling. *Knowledge-Based Systems* 236, 107729.
- [30] Nafa, Y., Chen, Q., Hou, B., Li, Z., 2024. Adaptive deep learning for entity disambiguation via knowledge-based risk analysis. *Expert Systems with Applications* 238, 122342.
- [31] News, W., 2023. Who launches new roadmap on breast cancer. <https://www.who.int/news/item/03-02-2023-who-launches-new-roadmap-on-breast-cancer>. [cited 3 February 2023].
- [32] Pati, P., Jaume, G., Fernandes, L.A., Foncubierto-Rodríguez, A., Feroce, F., Anniciello, A.M., Scognamiglio, G., Brancati, N., Riccio, D., Di Bonito, M., et al., 2020. Hact-net: A hierarchical cell-to-tissue graph neural network for histopathological image classification, in: *Uncertainty for Safe Utilization of Machine Learning in Medical Imaging, and Graphs in Biomedical Image Analysis: Second International Workshop, UNSURE 2020, and Third International Workshop, GRAIL 2020, Held in Conjunction with MICCAI 2020, Lima, Peru, October 8, 2020, Proceedings 2*, Springer. pp. 208–219.
- [33] Pati, P., Jaume, G., Foncubierto-Rodríguez, A., Feroce, F., Anniciello, A.M., Scognamiglio, G., Brancati, N., Fiche, M., Dubruc, E., Riccio, D., et al., 2022. Hierarchical graph representations in digital pathology. *Medical image analysis* 75, 102264.
- [34] Pereyra, G., Tucker, G., Chorowski, J., Kaiser, L., Hinton, G., 2017. Regularizing neural networks by penalizing confident output distributions. *arXiv preprint arXiv:1701.06548* .
- [35] Raffel, C., Shazeer, N., Roberts, A., Lee, K., Narang, S., Matena, M., Zhou, Y., Li, W., Liu, P.J., 2020. Exploring the limits of transfer learn-

- ing with a unified text-to-text transformer. *The Journal of Machine Learning Research* 21, 5485–5551.
- [36] Rebuffi, S.A., Kolesnikov, A., Sperl, G., Lampert, C.H., icarl, . Incremental classifier and representation learning, in: *Conference on Computer Vision and Pattern Recognition (CVPR)*, pp. 5533–5542.
 - [37] Sajid, U., Khan, R.A., Shah, S.M., Arif, S., 2023. Breast cancer classification using deep learned features boosted with handcrafted features. *Biomedical Signal Processing and Control* 86, 105353.
 - [38] Selvaraju, R.R., Cogswell, M., Das, A., Vedantam, R., Parikh, D., Batra, D., 2017. Grad-cam: Visual explanations from deep networks via gradient-based localization, in: *Proceedings of the IEEE international conference on computer vision*, pp. 618–626.
 - [39] Srinidhi, C.L., Ciga, O., Martel, A.L., 2021. Deep neural network models for computational histopathology: A survey. *Medical Image Analysis* 67, 101813.
 - [40] Stegmüller, T., Bozorgtabar, B., Spahr, A., Thiran, J.P., 2023. Scorenet: Learning non-uniform attention and augmentation for transformer-based histopathological image classification, in: *Proceedings of the IEEE/CVF Winter Conference on Applications of Computer Vision*, pp. 6170–6179.
 - [41] Vang, Y.S., Chen, Z., Xie, X., 2018. Deep learning framework for multi-class breast cancer histology image classification, in: *Image Analysis and Recognition: 15th International Conference, ICIAR 2018, Póvoa de Varzim, Portugal, June 27–29, 2018, Proceedings 15*, Springer. pp. 914–922.
 - [42] Vaswani, A., Shazeer, N., Parmar, N., Uszkoreit, J., Jones, L., Gomez, A.N., Kaiser, Ł., Polosukhin, I., 2017. Attention is all you need. *Advances in neural information processing systems* 30.
 - [43] Veta, M., Pluim, J.P., Van Diest, P.J., Viergever, M.A., 2014. Breast cancer histopathology image analysis: A review. *IEEE transactions on biomedical engineering* 61, 1400–1411.

- [44] Wang, X., Yang, S., Zhang, J., Wang, M., Zhang, J., Huang, J., Yang, W., Han, X., 2021. Transpath: Transformer-based self-supervised learning for histopathological image classification, in: Medical Image Computing and Computer Assisted Intervention–MICCAI 2021: 24th International Conference, Strasbourg, France, September 27–October 1, 2021, Proceedings, Part VIII 24, Springer. pp. 186–195.
- [45] Wang, X., Yang, S., Zhang, J., Wang, M., Zhang, J., Yang, W., Huang, J., Han, X., 2022. Transformer-based unsupervised contrastive learning for histopathological image classification. *Medical image analysis* 81, 102559.
- [46] Yan, R., Ren, F., Li, J., Rao, X., Lv, Z., Zheng, C., Zhang, F., 2022. Nuclei-guided network for breast cancer grading in he-stained pathological images. *Sensors* 22, 4061.
- [47] Younker Hyde Macfarlane, P., 2018. Cancer misdiagnosis: When should it be caught? URL: <https://www.patientinjury.com/blog/2018/01/29/cancer-misdiagnosis-when-should-it-187801>.
- [48] Yu, G., Chen, Z., Wu, J., Tan, Y., 2021. A diagnostic prediction framework on auxiliary medical system for breast cancer in developing countries. *Knowledge-Based Systems* 232, 107459.
- [49] Zadrozny, B., Elkan, C., 2002. Transforming classifier scores into accurate multiclass probability estimates, in: Proceedings of the eighth ACM SIGKDD international conference on Knowledge discovery and data mining, pp. 694–699.
- [50] Zerouaoui, H., Idri, A., 2022. Deep hybrid architectures for binary classification of medical breast cancer images. *Biomedical Signal Processing and Control* 71, 103226.
- [51] Zhang, L., Lu, X., Chen, Z., Liu, T., Chen, Q., Li, Z., 2022. Adaptive deep learning for network intrusion detection by risk analysis. *Neurocomputing* 493, 46–58.
- [52] Zhuang, F., Qi, Z., Duan, K., Xi, D., Zhu, Y., Zhu, H., Xiong, H., He, Q., 2020. A comprehensive survey on transfer learning. *Proceedings of the IEEE* 109, 43–76.